Neuron, Vol. 34, 715–727, May 30, 2002, Copyright ©2002 by Cell Press

Disruption of Dynein/Dynactin Inhibits Axonal Transport in Motor Neurons Causing Late-Onset Progressive Degeneration

Bernadette H. LaMonte,[1] Karen E. Wallace,[1] Beth A. Holloway,[1] Spencer S. Shelly,[1] Jennifer Ascaño,[1] Mariko Tokito,[1] Thomas Van Winkle,[2] David S. Howland,[3] and Erika L.F. Holzbaur[1,4]

[1]Department of Physiology
School of Medicine and
Department of Animal Biology
University of Pennsylvania
3700 Hamilton Walk

[2]Department of Pathobiology
School of Veterinary Medicine
University of Pennsylvania
300 Spruce Street
Philadelphia, Pennsylvania 19104

[3]Wyeth Research
865 Ridge Road
Princeton, New Jersey 08543

Summary

To test the hypothesis that inhibition of axonal transport is sufficient to cause motor neuron degeneration such as that observed in amyotrophic lateral sclerosis (ALS), we engineered a targeted disruption of the dynein-dynactin complex in postnatal motor neurons of transgenic mice. Dynamitin overexpression was found to disassemble dynactin, a required activator of cytoplasmic dynein, resulting in an inhibition of retrograde axonal transport. Mice overexpressing dynamitin demonstrate a late-onset progressive motor neuron degenerative disease characterized by decreased strength and endurance, motor neuron degeneration and loss, and denervation of muscle. Previous transgenic mouse models of ALS have shown abnormalities in microtubule-based axonal transport. In this report, we describe a mouse model that confirms the critical role of disrupted axonal transport in the pathogenesis of motor neuron degenerative disease.

Introduction

Motor neurons of the brain and spinal cord are uniquely characterized by the length of their axons, which can reach a meter in length in an adult human. The significant length of these cellular projections makes active axonal transport essential for normal cellular function. This axonal transport is microtubule dependent and includes both the anterograde transport of organelles to the synapse and the retrograde transport of multivesicular bodies and trophic factors such as NGF back to the cell body.

Motor neuron degenerative diseases affect most mammals. In humans, amyotrophic lateral sclerosis (ALS) is a progressive degenerative disorder of motor neurons in the cortex, brainstem, and spinal cord (for reviews, see Borchelt et al., 1998; Cleveland, 1999; Julien, 2001). ALS is a late onset disease that is characterized by progressive muscle weakness that leads to paralysis and eventual death. Currently, there is no known cure or effective treatment for this devastating disease, which has an incidence of roughly 5 in 200,000 people. Approximately 5%–10% of ALS cases are familial (FALS), and of these, 15%–20% have a missense mutation in the gene for Cu/Zn superoxide dismutase I (Rosen et al., 1993). Mutations in the heavy subunit of neurofilaments (Julien, 1997) and the GTPase alsin (Yang et al., 2001) have also been linked to rare cases of ALS, but the genetic defect or defects responsible for the majority of FALS have not yet been identified. The possible causes of sporadic ALS, which is clinically indistinguishable from FALS, are unknown, but environmental factors have been implicated. The wide variety of factors, both known and unknown, that cause the similar and specific degeneration of motor neurons has made it difficult to understand the pathogenesis of this disease.

One hallmark of motor neuron degeneration observed in both affected ALS patients and transgenic mice expressing the SOD-1 mutation is the accumulation of neurofilaments (NFs) in the perikarya and axons of motor neurons (for review, see Julien, 2001). These cells have large caliber axons dependent on neurofilament proteins for the maintenance of their structure (Xu, et al., 1996, Elder et al., 1998a, 1998b). Neurofilaments, like other components of the cytoskeleton, are continually renewed and require transport from the cell body, where they are synthesized, into and throughout the axon. These large filaments are normally transported by microtubule-based anterograde transport at a rate an order of magnitude slower than the rate of organelle transport. The aberrant accumulation of neurofilament proteins has been implicated in the development of motor neuron degenerative diseases but may also be an indication of abnormal transport of these large proteins (Julien, 2001).

Several transgenic mouse lines that display a motor neuron degenerative phenotype have been shown to exhibit significant defects in axonal transport. Decreased rates of slow axonal transport have been shown in mice expressing mutant SOD-1 (Collard et al., 1995; Zhang et al., 1997; Williamson and Cleveland, 1999). It has been postulated that defects in axonal transport may be an underlying common pathway that leads to the degeneration of motor neurons in ALS patients and transgenic mouse models. In the SOD models, misfolding of the mutant SOD-1 protein confers a unique cytotoxic property that may affect the transport machinery either directly or indirectly. Neurofilament accumulation in transport-deficient axons may then effectively impede further transport along microtubules, leading to motor neuron degeneration through "axonal strangulation" (Williamson and Cleveland, 1999).

Cytoplasmic dynein is a molecular motor responsible for minus-end-directed movement along microtubules. It is involved in many cellular functions including ER to Golgi trafficking and mitotic spindle assembly. In neurons, dynein has an essential role in fast retrograde axonal transport (Paschal and Vallee, 1987; Hirokawa et

[4]Correspondence: holzbaur@mail.med.upenn.edu

al., 1990) as well as in the targeting of developing neurons (Reddy et al., 1997). Dynein has also been proposed to be a participant in slow anterograde axonal transport (Dillman et al., 1996), but the mechanism remains elusive. The slow anterograde transport of neurofilaments may at least in part be dependent on the retrograde molecular motor dynein and the associated protein complex, dynactin (Shah et al., 2000; Wang et al., 2000).

Dynactin is a multiprotein complex associated with dynein. Dynactin has been proposed to activate the motor function of dynein by increasing the processivity and efficiency of the motor (Waterman-Storer, et al., 1995; King and Schroer, 2000). Dynactin also participates in cargo binding (Waterman-Storer et al., 1997; Starr et al., 1998; Holleran et al., 2001; Muresan et al., 2001). The largest subunit of dynactin, p150^{Glued}, binds to both microtubules and the intermediate chain of dynein (Waterman-Storer et al., 1995; Karki and Holzbaur, 1995). The base of dynactin consists of the Arp1 filament, which has been shown to bind to the spectrin matrix found on organelles and therefore may mediate cargo attachment (Holleran et al., 1996, 2001; Muresan et al., 2001). Overexpression of the dynamitin (p50) subunit of dynactin causes a dissociation of dynactin at the junction of p150^{Glued} and the Arp1 filament (Echeverri et al., 1996; Eckley et al., 1999). This effectively renders dynactin nonfunctional (Echeverri et al., 1996) and has been shown to inhibit dynein-mediated processes in the cell (Presley et al., 1997; Burkhardt et al., 1997). Thus, dynamitin overexpression is a powerful tool in dissecting the roles of dynein and dynactin in the cell.

To directly test the hypothesis that inhibition in axonal transport may be sufficient to cause motor neuron degeneration similar to that observed in ALS, we engineered a targeted disruption of the dynein-dynactin complex in postnatal motor neurons of transgenic mice. Mice overexpressing dynamitin demonstrate a late-onset, slowly progressive motor neuron degenerative disease characterized by muscle weakness, spontaneous trembling, abnormal posture and gaits, and deficits in strength and endurance. Dynamitin-overexpressing mice have histological changes in spinal cord motor neurons and skeletal muscle indicative of degeneration of motor neurons and denervation atrophy of muscle. These mice display neurofilament accumulations and a significant inhibition of retrograde transport. Previous ALS transgenic mouse models have shown abnormalities in microtubule based axonal transport. Here we describe a mouse model that confirms the critical role of disrupted axonal transport in the development of motor neuron degenerative diseases.

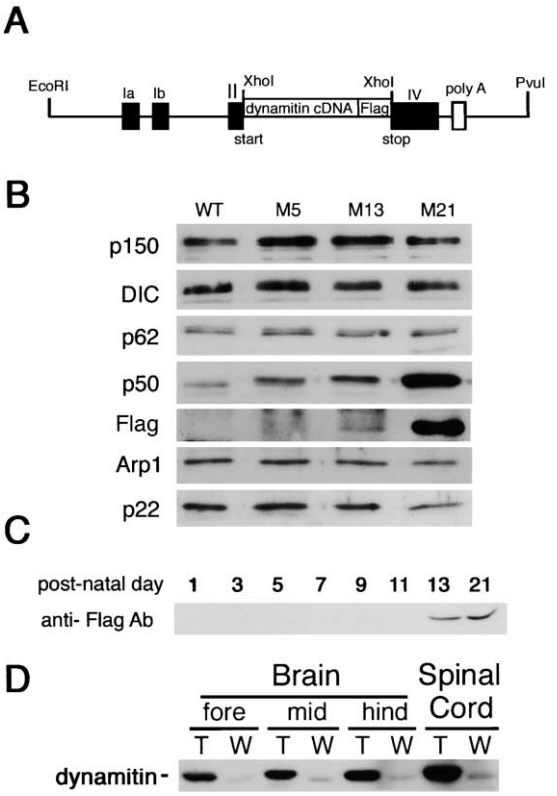

Figure 1. Generation and Characterization of Transgenic Mice Overexpressing Dynamitin

(A) Construct used to generate dynamitin transgenic mice. An EcoRI-PvuI fragment of the Thy1.2 expression cassette contains sequences essential for expression (Caroni, 1997). Human dynamitin cDNA with a FLAG tag was cloned into the XhoI site of the expression cassette.

(B) Western blot analysis. Equal amounts of spinal cord total protein extracts from mice of three founder lines, M5, M13, M21, and wild-type mice were resolved by SDS-PAGE, and a Western blot was done with dynein and the dynactin subunits. The highest dynamitin expression levels were observed in the M21 line, as expected from the RNase protection study.

(C) Onset of expression in transgenic mice. Brain homogenates from mouse pups of the M21 line, sacrificed at the indicated time points after birth, were analyzed by SDS-PAGE and Western blot using antibodies specific for the FLAG tag to determine onset of expression at the protein level. Transgenic expression was observed at day 13 in M21 mice.

(D) Expression of dynamitin in transgenic mouse tissues. Homogenates from brain that had been divided into three equal parts rostral to caudal on gross dissection and spinal cord samples were analyzed by SDS-PAGE and Western blot using an affinity-purified antibody to dynamitin. Highest expression levels were seen in the spinal cord.

Results

Generation and Characterization of Transgenic Mice Overexpressing Dynamitin in Motor Neurons

To examine the functional consequence of disrupting dynein-mediated axonal transport in the development of neurodegenerative diseases, we developed three lines of transgenic mice that overexpress the dynamitin subunit of dynactin. Overexpression of this polypeptide has previously been demonstrated to disrupt dynein function in cell division (Echeverri et al., 1996), vesicle trafficking (Presley et al., 1997), organelle localization (Burkhardt et al., 1997), and axonal outgrowth in cultured cells (Ahmed et al., 1998). The Thy1.2 expression cassette was used to drive dynamitin expression because of its specific high expression in postnatal motor neurons (Caroni, 1997). A FLAG tag was added to the C terminus of dynamitin to facilitate identification of transgenic versus endogenous dynamitin (Figure 1A). Three founder mice were identified and bred to establish three separate lines of dynamitin-overexpressing transgenic mice.

RNase protection assays on brain tissue were used

to quantify the levels of dynamitin overexpression in the transgenic mouse lines (data not shown). Two lines (M5 and M13) had ~2- to 4-fold increased levels of dynamitin mRNA. In contrast, the M21 line was estimated to have an ~20-fold increase in dynamitin mRNA levels. Because of these higher expression levels, we chose to focus on this line for further study.

In order to examine the expression of dynamitin at the protein level, Western blots of spinal cord homogenates from the three transgenic lines as well as age-matched wild-type controls were probed with antibodies to dynamitin (Figure 1B). As expected from the RNase protection results, the M21 line was observed to have the highest levels of dynamitin expression. Western blots were also probed with antibodies to other dynactin subunits, including p150^{Glued}, p62, Arp1, and p22, to examine the relative expression of these polypeptides in the transgenic lines as compared to wild-type mice (Figure 1B). No significant differences were noted in the expression of p150^{Glued}, p62, and Arp1 among any of the transgenic lines. p22 expression was observed to be more variable and may be affected by the expression of the transgene.

A critical feature of the Thy1.2 expression cassette is that the onset of expression occurs ~6–10 days after birth (Caroni, 1997). We predicted that this delay in onset of expression should allow us to distinguish effects of dynamitin overexpression during embryogenesis from postnatal effects that may more closely resemble late-onset degenerative diseases. This was important because dynein and dynactin function are known to be required for the normal development of neurons and the assembly of neural circuitry in *Drosophila* (Murphey et al., 1999; Reddy et al., 1997). In addition, transgenic mice with a null mutation in dynein die in utero (Harada et al., 1998).

To determine the onset of transgene expression, a time course study was performed. M21 pups were sacrificed at postnatal days 1, 3, 5, 7, 9, 11, 13, and 21, and brain homogenates were prepared. Western blots of the homogenates were then probed with antibodies to the FLAG tag. Expression of the transgene in the M21 line was not observed until postnatal day 13 (Figure 1C), suggesting that abnormalities seen in these transgenic mice are due to the effects of disrupted dynein function on mature neurons, rather than from disruptive effects during motor neuron development. Histological analysis of the transgenic mice, which revealed no gross perturbations or abnormalities in the anatomy or organization of the nervous system, also supports this conclusion.

Western blots of all major tissue types from M21 mice and age-matched controls were examined to analyze the tissue specificity of transgene expression. Dynactin is enriched in nervous and muscle tissue; therefore, endogenous expression of dynamitin is observed in these tissues (Melloni et al., 1995). In skeletal muscle, there is no significant difference in the levels of dynamitin expression between transgenic and control mice (data not shown). Transgenic mice display the highest expression of dynamitin in neuronal tissues, particularly the spinal cord and hindbrain, as compared to control mice (Figure 1D). No significant differences in dynamitin expression between transgenic and wild-type mice were observed in any tissue examined other than those from the nervous system (data not shown). This pattern of expression is in agreement with previous reports that Thy1.2-driven transgene expression in the mouse is restricted to neurons (Caroni, 1997; Feng et al., 2000).

Disruption of Dynactin in Motor Neurons

Dynein and dynactin sediment with characteristically large S values (19S–20S). Overexpression of dynamitin results in a shift of dynactin subunits to lower S values due to the disassembly of the complex into two fractions; Arp1 and p62 remain in one fraction while p150^{Glued}, p22, and dynamitin are in another (Echeverri et al., 1996). In order to examine the effectiveness of dynamitin overexpression in disrupting dynactin in the neurons of transgenic mice, high-speed cytosolic extracts of spinal cord preparations from 5-month-old presymptomatic mice and wild-type control mice were fractionated by sucrose density gradients (Figure 2). Disruption of the dynactin complex is indicated by the shift of p150^{Glued}, dynamitin, and p22 to lower density fractions. Arp1 and p62 are shifted by a single fraction, consistent with previous observations (Echeverri et al., 1996; Eckley et al., 1999). In wild-type controls, the peak concentration of dynactin subunits from wild-type spinal cord extracts remains at 19S–20S. The disruption of dynactin we observed in transgenic mouse spinal cord relative to controls was extensive, but not complete, most likely due to the specificity of the Thy1.2 expression cassette for motor neurons. Previous studies with this promoter reveal only limited expression in other neuronal populations in the spinal cord and none in glial cells (Caroni, 1997). Further, the immunohistochemistry results described below indicate that high levels of dynamitin overexpression are not observed in all spinal cord motor neurons of M21 mice (see Figure 5).

Mice Overexpressing Dynamitin Display Evidence of Motor Neuron Degeneration and Skeletal Muscle Atrophy

The onset of disease in transgenic mice from the M21 line begins between 5 and 9 months of age (Figure 3A). The severity and progression of the symptoms is variable between littermates, but most M21 mice display hind end weakness, spontaneous and sometimes spastic tremors, decreased grooming, weight loss, decreased fertility, and abnormal gaits. Mice also lose the ability to extend their hind legs when suspended by the base of their tail. A less severe phenotype with similar symptoms of hind end weakness, abnormal gaits, and trembling is observed in the lower expressing M5 and M13 mouse lines. These milder signs do not develop until 14–18 months of age.

Many transgenic mice of the M21 line exhibit abnormal gaits. Some mice appear to be lame on a limb, or their posture is slumped in the hind end. A small number of transgenic mice become weak in their epaxial muscles and develop a lordodic posture with an upright tail. Transgenic mice develop abnormal, slower gaits with decreased stride lengths, which can be demonstrated by ink tests (see Figure 3C). Mice with signs of weakness also had decreased fertility. Males did not become sick enough to prevent them from fertilizing females until they reached the severe stages of the disease. Females, on the other hand, were not able to successfully raise litters once they began to show signs of disease.

Transgenic mice become weak and have difficulty

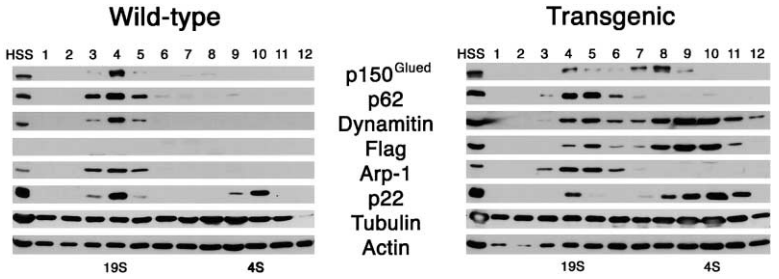

Figure 2. Disruption of Dynactin In Vivo by Overexpressed Dynactin

Homogenates of spinal cord preparations from 5-month-old wild-type and transgenic mice were sedimented on 5%–20% sucrose gradients. Fractions were resolved by SDS-PAGE, and Western blot was performed using antibodies specific for the dynactin subunits p150^{Glued}, p62, dynamitin, Arp1, and p22 as well as antibodies to the FLAG tag and to tubulin and actin. Standards were run in parallel to determine relative densities of fractions. HSS is pre-load high-speed supernatant from mouse spinal cord homogenates. Disruption of the dynactin multiprotein complex is demonstrated by the shift of subunits into lower density fractions. p150^{Glued}, dynamitin, and p22 divide into a subcomplex that sediments at ~4S while Arp1 and p62 shift one fraction from 4 to 5.

climbing on wire mesh, are not as active in the cage, and display decreased rearing activity. In order to assess the weakness that develops in dynamitin-overexpressing mice, analysis of 4- to 7-month-old presymptomatic transgenic and wild-type male mice, 10- to 14-month-old early symptomatic transgenic and wild-type male mice, and >17-month-old late symptomatic transgenic and wild-type male mice by grip strength meter (Meyer et al., 1979; Zhao et al., 2001) was performed. Late symptomatic transgenic mice exhibit a statistically significant ($p < 0.01$) decrease in forelimb strength when compared to age matched controls (Figure 3E).

Transgenic mice appear to tire easily on the grip strength meter and when suspended by their tails, so we tested for a decrease in endurance. Treadmill tolerance tests that tested time to refusal at slow and moderate treadmill speeds were performed on 4- to 7-month-old presymptomatic transgenic and wild-type male mice, 10- to 14-month-old early symptomatic transgenic and wild-type male mice, and >17-month-old late symptomatic transgenic and wild-type male mice. This protocol was designed to test the endurance of the animal rather than the maximum speed that it could run. Early symptomatic transgenic mice tire on average 44 min earlier than wild-type mice in the same age group ($p < 0.02$) during treadmill tolerance tests. Late symptomatic transgenic mice run on average 52 min less than the wild-type mice in the same age group ($p < 0.02$), indicating a decrease in stamina (Figure 3D).

Motor Neurons in Transgenic Mice Exhibit Neurofilament Accumulations

Four- to seven-month-old presymptomatic transgenic and wild-type, 10- to 14-month-old early symptomatic

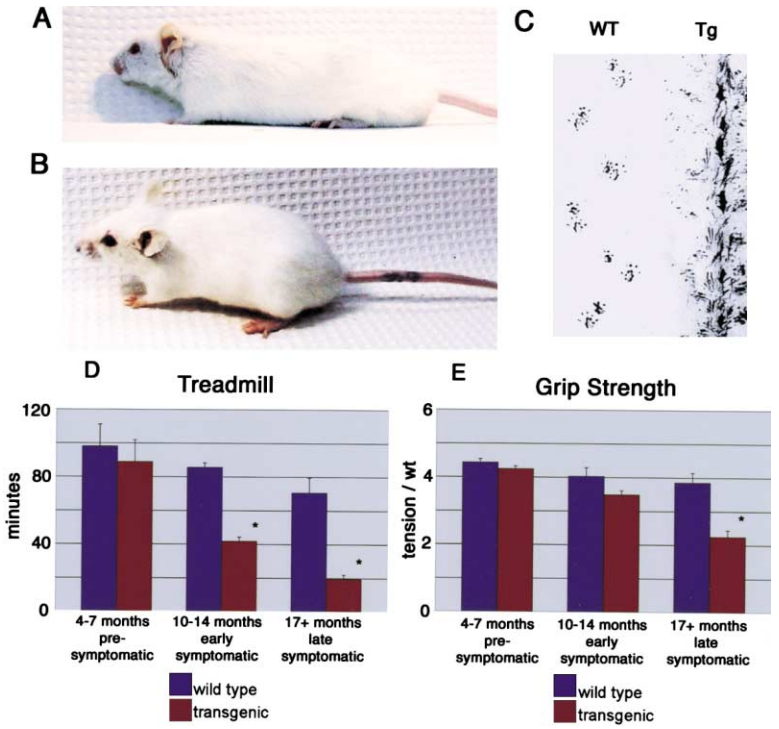

Figure 3. Dynamitin Transgenic Mice Display a Phenotype Consistent with a Motor Neuron Degenerative Disease

(A) Late symptomatic, dynamitin-overexpressing mouse. Transgenic M21 mice are weak, especially in the hind end, have abnormal gaits, lose the hind leg extension reflex, and often spontaneously tremble.

(B) Age-matched negative mouse.

(C) Dynamitin-overexpressing mice have decreased stride length and gait abnormalities. Wild-type versus late symptomatic transgenic mice were sent through a one-directional chute with painted feet to demonstrate stride abnormalities.

(D) Early and late symptomatic transgenic mice tire before age-matched negatives on treadmill endurance tolerance tests. Mice were exercised on a mouse treadmill at slow to moderate speeds in order to compare their stamina. Early and late symptomatic transgenic mice tire more than 40 min earlier than their age-matched wild-type controls. Shown are mean running times ± SE (t test, *$p < 0.02$).

(E) Early and late symptomatic transgenic mice demonstrate decreased strength on a grip strength meter. Forelimb strength was determined by averaging three trials after force exerted on the meter was corrected for mouse weight. Late symptomatic transgenic mice are significantly weaker than age-matched controls. Mean kg force/kg weight ± SE (t test, *$p < 0.001$).

transgenic and wild-type, and >17-month-old late symptomatic transgenic and wild-type mice spinal cord cross-sections from the lumbar intumescence were stained with hemotoxylin and eosin (H&E). In presymptomatic and early symptomatic transgenic mice not exhibiting clinical signs of disease, no gross anatomical or significant histological changes were observed in the brains or spinal cords (data not shown). In the early stages of the disease, significant degenerative changes would be expected to be seen at the distal end of axons, which are most dependent on transport. In presymptomatic and early symptomatic mice, no loss of motor neurons nor inclusions in cell bodies or processes were observed, and only very minor, subtle histological changes such as swollen axons were seen in early symptomatic mice. Histological changes were evident in >17-month-old late symptomatic transgenic mice when compared to wild-type mice in the same age group (Figures 4A and 4B). Degeneration and moderate loss of motor neurons are seen in the ventral horns of dynamitin-overexpressing mice (Figure 4B, inset). Transgenic sections have a spongiform appearance with debris in areas of possible cellular loss (Figure 4B, white arrow). Loss of axons is evident in the long tracks of spinal cord white matter (Figure 4B, black arrow). The loss of motor neurons was also confirmed by examining the number of axons seen in L5 ventral roots (see Figure 6). Swollen axons are also seen (Figure 4B, white arrowheads), resembling the spheroids described in the spinal cord of ALS patients.

Skeletal muscle was examined from whole limbs and epaxials from 4- to 7-month-old presymptomatic transgenic and wild-type, 10- to 14-month-old early symptomatic transgenic and wild-type, and >17-month-old late symptomatic transgenic and wild-type mice. As with other tissues examined, no significant abnormalities are seen in the pre- and early symptomatic mice, but abnormalities are observed in the late symptomatic transgenic mice (Figures 4C and 4D). Widespread evidence of denervation atrophy and regeneration is seen, but is most pronounced in the large hind limb flexors such as the biceps femoris. Obvious histological changes such as small angular fibers (Figure 4D, black arrows) indicating denervation, centrally placed nuclei (Figure 4D, arrowheads), and hypertrophic fibers (Figure 4D, asterisk) were observed. Changes in muscle fibers are seen in small groups, suggesting that previous events of denervation and reinnervation by neighboring motor neurons have occurred (Figure 4D, white arrow).

Initial screening for dynamitin expression and evidence of disrupted transport in early symptomatic transgenic mice at the onset of phenotype compared to age-matched controls was done by immunohistochemistry using antibodies to dynamitin, neurofilaments, and synaptophysin. Ten- to fourteen-month-old early symptomatic transgenic and wild-type mice were examined. Sections of fore-, mid-, and hindbrain as well as cervical, thoracic, and lumbar spinal cord were screened. Sections of brain showed limited expression of dynamitin in transgenic mice and no unusual staining of neurofilaments or synaptophysin (data not shown). Spinal cord motor neurons in the ventral horn of early symptomatic transgenic mice stained intensely for dynamitin (Figures 5D, 5J, and 5P), but not in age-matched controls (Figures 5A, 5G, and 5M). It should be noted that even though there was intense staining of dynamitin in spinal cord motor neurons, not every motor neuron was expressing dynamitin, consistent with previously observed expression patterns driven by the Thy1.2 promoter (Feng et al., 2000).

Neurofilament staining was examined to determine if disruption of the dynactin complex affects neurofilament distribution. Overall, neurofilament staining was more intense in spinal cord sections of early symptomatic transgenic mice (Figures 5E, 5K, and 5Q) compared to age-matched negatives (Figures 5B, 5H, and 5N). Neuronal processes are swollen with neurofilaments, and spheroids, similar to those seen with H&E, stain for neurofilaments (Figure 5Q). The neurofilament antibody used recognizes only phosphorylated heavy and light subunits, so as expected, neurofilament staining was not observed in the cell bodies of motor neurons. Peripheral nerves containing motor neuron fibers from transgenic mice also have higher accumulations of neurofilaments as compared to wild-type mice (data not shown).

Sections of brain and spinal cord were also stained with synaptophysin as a marker for axonal transport. Synaptophysin is a ubiquitous membrane protein associated with small synaptic vesicles and is present in all synaptic terminals (Navone et al., 1986). In a recent study, dynein and synaptophysin were found to partially colocalize and accumulate at both the proximal and distal ends of a nerve injury crush (Li et al., 2000). Consistent with a defect in axonal transport, accumulation of synaptophysin was seen at the periphery of neurons in the ventral horn of spinal cord sections of early symptomatic transgenic mice (Figures 5F, 5L, and 5R) as compared to the distribution of synaptophysin in control mice (Figures 5C, 5I, and 5O).

Examination of L5 Ventral Roots by Electron Microscopy

To determine the effects of dynamitin overexpression on axonal numbers and caliber, L5 ventral roots of 4- to 7-month-old presymptomatic transgenic and wild-type mice, 10- to 14-month-old early symptomatic and wild-type mice, and >16-month-old late symptomatic and wild-type mice were examined by light and electron microscopy. Ventral roots are comprised primarily of myelinated axons originating from motor neurons and are an accurate reflection of their numbers. Four- to seven-month-old presymptomatic transgenic mice have 100% ± 5% of the total number of axons observed in wild-type mice of the same age group. Ten- to fourteen-month-old early symptomatic transgenic mice have 92% ± 4% of the total number of axons found in wild-type mice in the same age group. A decrease of 25% ± 6% was found in the average total number of axons counted in the >16-month-old late symptomatic transgenic mice when compared to wild-type mice of the same age group (t test, $p < 0.08$).

We then counted the number of small caliber (<5 μm in diameter) axons (SCAs) and large caliber (>5 μm in diameter) axons (LCAs) in 4- to 7-month-old presymptomatic, 10- to 14-month-old early symptomatic, and >16-month-old late symptomatic mice to determine if one population of axons was selectively vulnerable to the effects of transgene expression. 4- to 7-month-old presymptomatic transgenic mice have no significant dif-

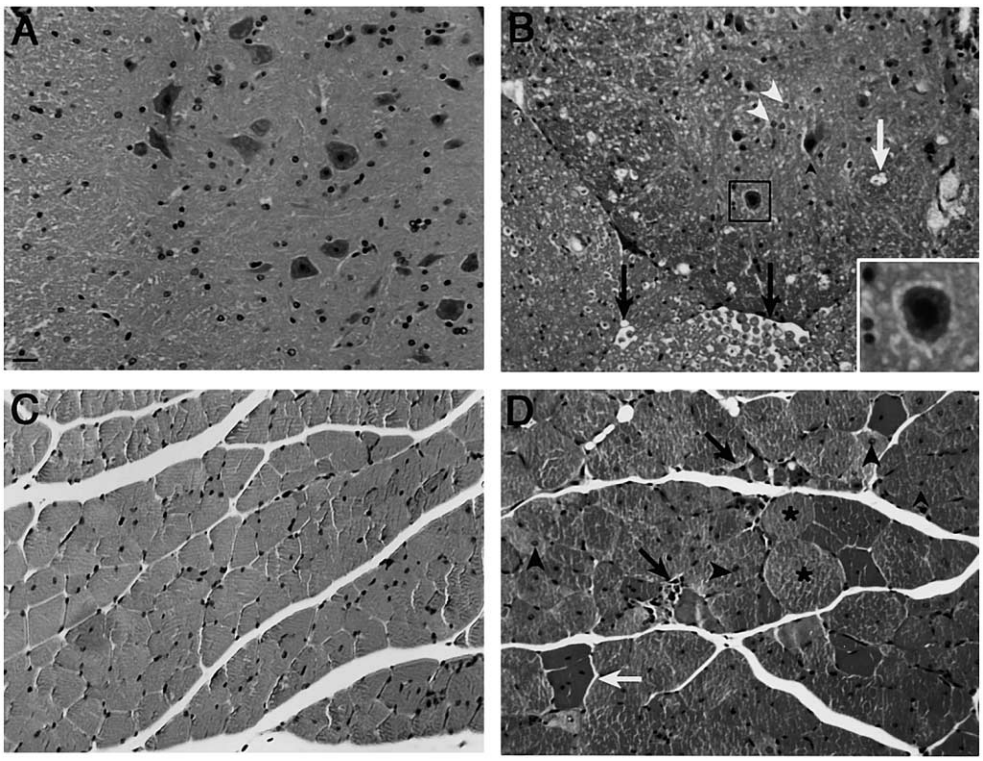

Figure 4. Hemotoxilin and Eosin Staining of Transgenic and Age-Matched Wild-Type Mouse Spinal Cord and Skeletal Muscle Tissue Sections

(A) Ventral horn of spinal cord cross-section from lumbar intumescence of a 14-month-old wild-type mouse. Note the large motor neuron cell bodies in the ventral horn, which is bordered by white matter.

(B) Ventral horn of spinal cord cross-section from approximately the same region of a 14-month-old symptomatic transgenic mouse. Fewer motor neuron cell bodies are seen, as quantified by counting axons in the L5 ventral root (see Figure 6). The spongiform appearance of gray matter with debris also indicates cellular loss (white arrow). Some degenerate motor neurons are seen (see vacuolations of cell body in insert). Swollen axons or spheroids are observed (white arrowheads), as well as loss of white matter in the long spinal tracts (black arrow).

(C) Cross-section of muscle from the large hind limb flexors (biceps femoris) of the age-matched wild-type mouse in (A).

(D) Cross-section of the same muscle from the symptomatic transgenic mouse in (B). Muscle fiber central nuclei (black arrowhead) and small angular fibers (black arrow) indicate degeneration and atrophy from denervation. Clusters of muscle fibers undergoing similar changes (white arrow) demonstrate a conversion from the normal heterogeneous innervation. Compensatory hypertrophy of muscle fibers (asterisk) is also seen. Scale bar is 20 μm.

ferences in the number of the SCAs (98% ± 3%) and LCAs (101% ± 1%) when compared to wild-type mice in the same age group. Ten- to fourteen-month-old early symptomatic transgenic mice have 96% ± 4% of the SCAs and 90% ± 4% of the LCAs of wild-type mice in the same age group. A significant decrease (t test, $p < 0.02$) was found in the number of LCAs of >16-month-old late symptomatic transgenic mice when compared to >16-month-old wild-type mice. Late symptomatic transgenic mice have 99% ± 2% of SCAs but only 65% ± 2% of the LCAs found in >16-month-old wild-type mice.

No abnormalities or significant differences are found in L5 ventral roots of 4- to 7-month-old presymptomatic transgenic mice (Figure 6B) when compared to wild-type mice (Figure 6A). In the 10- to 14-month-old early symptomatic transgenic mice (Figure 6D), an upward trend in the variability of axonal caliber is noted with no significant loss of axonal numbers when compared to wild-type mice in the same age group as described above (Figure 6C). This loss of axonal caliber size maintenance may be due to deficiencies in the slow transport of neurofilaments.

In the >16-month-old late symptomatic transgenic mice (Figure 6F), evidence of degeneration and axonal loss is seen when compared to wild-type mice of the same age group (Figure 6E). There are degenerate axons, axonal inclusions, myelin defects, and an increase in space between axons, suggesting axonal loss (Figure 6F). These observations are similar to those described in EM analysis of ventral roots in mutant SOD-1 mice (Bruijin et al., 1997). We also observed many axons with involutions or invaginations of the myelin sheath into the axons, indicating axonal atrophy and suggesting a deficient or collapsed cytoskeleton.

Delay in Retrograde Transport Observed in Early Symptomatic Transgenic Mice

In order to directly correlate the degenerate changes seen in motor neurons and their axons and the development of the observed phenotype in transgenic mice with disruptions in axonal transport, neurotracer studies were performed. Transgenic mice and age-matched wild-type controls were injected with the retrograde neurotracer fluoro-gold in the gastrocnemius muscle and sacrificed at 44 and 46 hr to determine the number

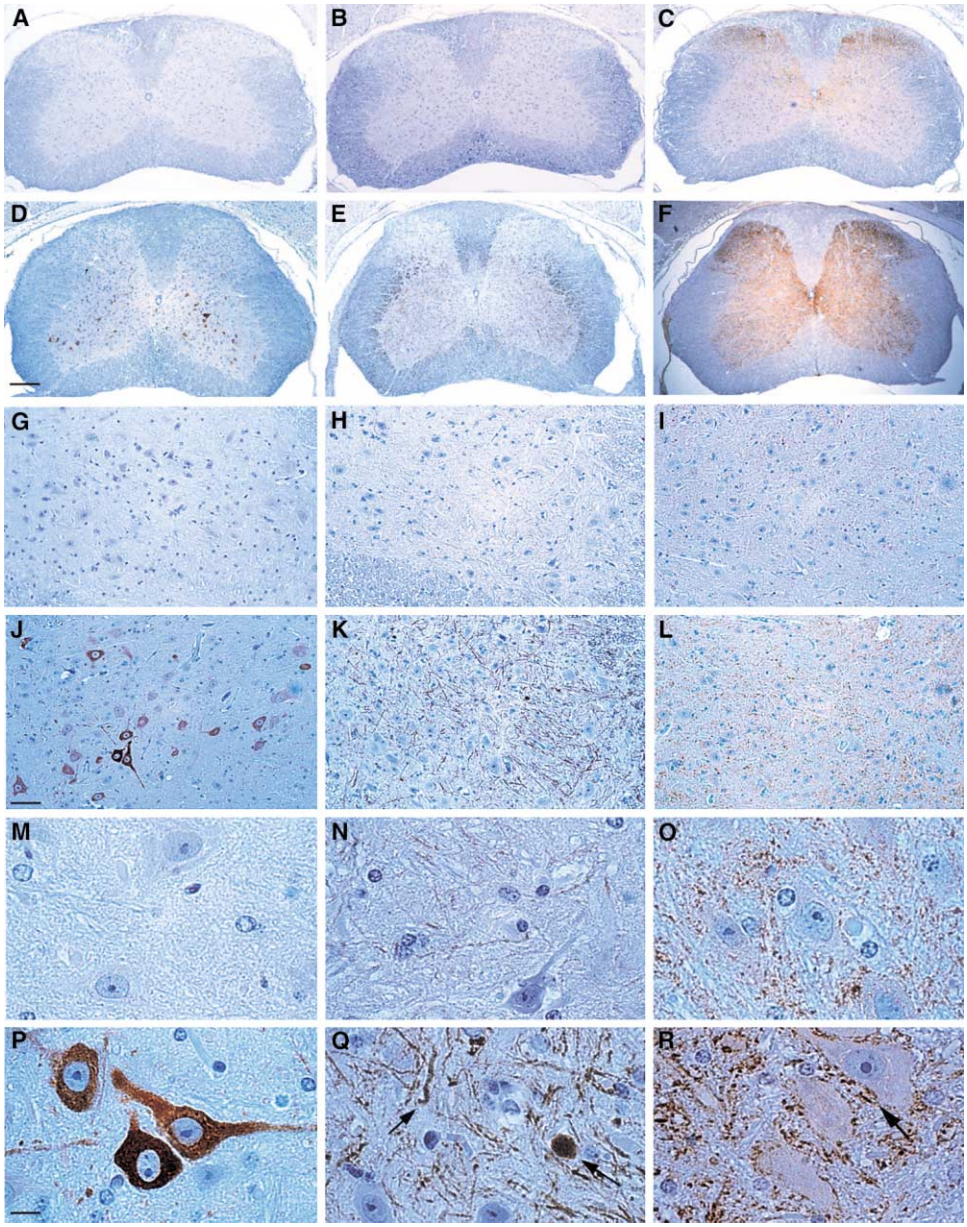

Figure 5. Immunohistochemistry of Spinal Cord Sections from Transgenic Mice.

Panels in the left column (A, D, G, J, M, and P) are stained for dynamitin, those in the center column (B, E, H, K, N, and Q) for phosphorylated neurofilaments, and those in the right column (C, F, I, L, O, and R) for synaptophysin. Panels (A), (B), (C), (G), (H), (I), (M), (N), and (O) are age-matched wild-type mice and panels (D), (E), (F), (J), (K), (L), (P), (Q), and (R) are from M21 transgenic mice. Panels (A)–(F) are 5× (scale bar = 200 μm), (G)–(L) are 20× (scale bar = 50 μm), and (M)–(S) are 100× (scale bar = 10 μm). Note the elevated and specific levels of dynamitin expression in motor neurons of the ventral horn in dynamitin-stained panels of transgenic mice (D, L, and P). Large aggregates of neurofilament in cell processes as well as axonal swellings (black arrows) are seen in (E), (K), and (Q). There is also increased staining for synaptophysin in transgenic mice (F and L) and accumulation at the cell periphery of motor neurons (black arrows in [R]). Sections from wild-type and transgenic mice were developed in parallel according to a fixed protocol.

of motor neuron cell bodies that had accumulated fluoro-gold (Schmued, 1994). No significant differences were detected in presymptomatic mice. Retrograde transport could not be quantitated in late symptomatic transgenic mice because of the significant loss of motor neurons found in this group. Therefore quantitation of transport deficits was performed on 10- to 14-month-old early symptomatic transgenic mice in comparison to wild-type controls.

Accumulation of the fluoro-gold neurotracer was observed in whole motor neuron pools that innervate the injected muscle at the 44 and 46 hr time points in wild-type mice and is demonstrated in Figure 7B. In contrast, transgenic mice in the same age group had only an occasional cell with fluoro-gold accumulation at the 44 and 46 hr time points (Figure 7A), while still possessing normal motor neuron numbers in this age group of mice (H&E results and Figure 7A, inset). These rare labeled

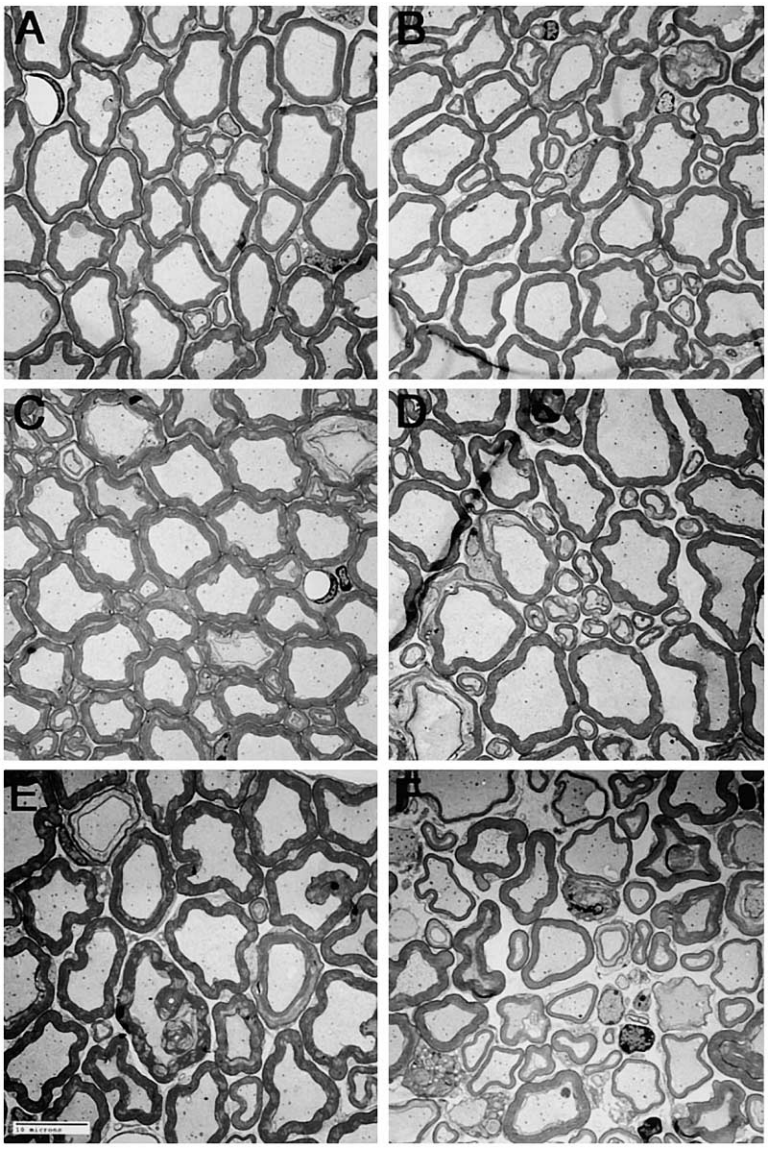

Figure 6. Electron Microscopy of Presymptomatic, Early Symptomatic, and Late Symptomatic Transgenic Mice and Age-Matched Wild-Type Mice

Representative electron microscopy images of L5 ventral roots in cross-section. There are no appreciable differences in appearance or number of axons in 4- to 7-month-old wild-type (A) and presymptomatic transgenic mice (B). 10- to 14-month-old wild-type (C) and age-matched early symptomatic transgenic mice (D) have similar numbers of axons, but there is a trend toward a larger variation in axonal caliber seen in early symptomatic transgenic mice. >16-month-old wild-type (E) and late symptomatic transgenic mice (F) have statistically different numbers of axons and considerable changes in their appearance. Late symptomatic transgenic mice have a dropout of 25% $\pm$ 6% in the total number of axons as compared to wild-type mice in the same age group (t test, $p < 0.08$). This correlates with a statistically significant (t test, $p < 0.02$) decrease in the number of large (>5 μm diameter) caliber axons of 35% $\pm$ 2% when compared wild-type mice in the same age group. Images from late symptomatic transgenic mice demonstrate increased space between axons, supporting axonal loss as well as degenerate axons, inclusions, and defects in myelination (F). Scale bar is 10 μm.

cells may correspond to motor neurons that do not overexpress dynamitin, as high levels of dynamitin were observed in only a subset of motor neurons (Figure 5).

At 44 hr, the average number of labeled cells per mouse is 46.5 $\pm$ 16.5 (average $\pm$ SE; n = 6) in wild-type mice, whereas the average number of labeled cells per mouse is 15.2 $\pm$ 8.5 (n = 4) in early symptomatic 10- to 14-month-old transgenic mice (p = 0.135). At 46 hr postinjection of fluoro-gold, a significant decrease of labeled cells was found in transgenic mice (Figure 7A) when compared to the accumulation observed in wild-type mice (Figure 7B). An average of 48.7 $\pm$ 7.4 (n = 6) labeled cells per wild-type mouse was found, whereas an average of only 16.0 $\pm$ 5.8 labeled cells per mouse was found in early symptomatic transgenic mice (t test, $p < 0.01$) (Figure 7C). At later time points, preliminary observations have shown that in transgenic mice, the fluoro-gold neurotracer accumulates in motor neuron pools more similarly to wild-type controls (data not shown), suggesting that dynamitin overexpression delays but does not completely block retrograde axonal transport.

Sciatic nerve ligations of symptomatic transgenic mice and age-matched controls were also performed to probe for possible differences in anterograde transport. However, over a 2–6 hr time course, no consistent, appreciable difference could be found between transgenic and wild-type mice. Given the relatively short time frame of this experiment and the limited overexpression of dynamitin to motor neurons within a mixed cell population in the sciatic nerve, definitive conclusions cannot be drawn about the possible effects of dynamitin overexpression on anterograde axonal transport. The significant inhibition of retrograde rather than anterograde transport in the transgenic mice is consistent with dynein's role as a minus-end-directed microtubule motor.

Discussion

Motor neuron degenerative diseases are severely debilitating and largely fatal in humans as well as other mammalian species. Several hypotheses have been proposed to explain the pathogenesis of these diseases,

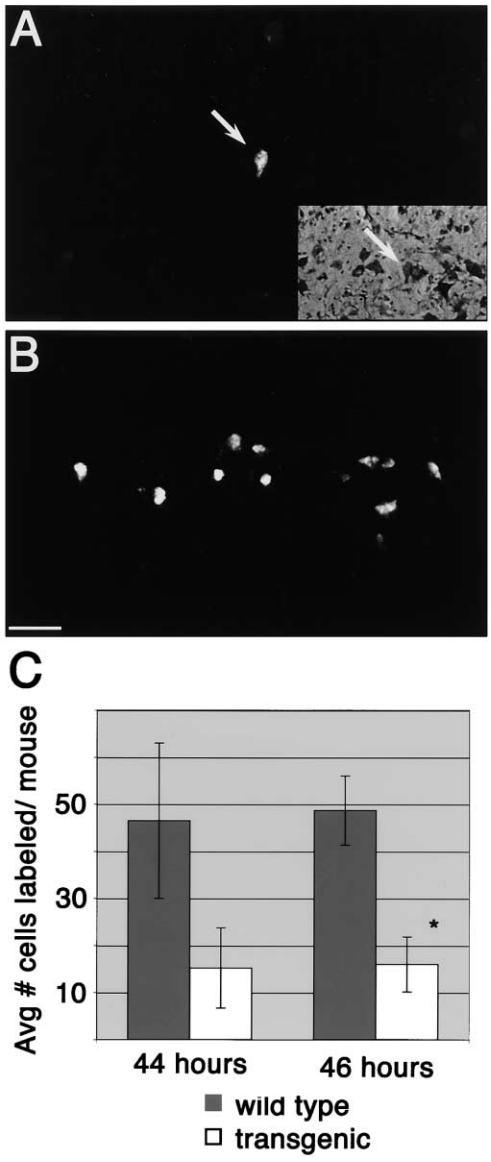

Figure 7. Early Symptomatic Mice Have a Decrease in the Number of Motor Neurons Labeled by the Retrograde Neuro-Tracer Fluoro-Gold

Longitudinal spinal cord section from the lumbar intumescence of a 10- to 14-month-old early symptomatic transgenic mouse injected with the retrograde neuro-tracer fluoro-gold and sacrificed at 46 hr postinjection (A). No accumulation in the cell bodies of motor neuron pools is seen except for a rare singly labeled cell. Counter stain of (A) to visualize motor neuron pool in spinal cord (A, inset). Longitudinal section of spinal cord from wild-type age-matched mouse sacrificed at 46 hr postinjection demonstrating accumulation of fluoro-gold in motor neuron pools (B). At 44 hr, an average of 31 more motor neurons in wild-type mice accumulate fluoro-gold than transgenic mice, and at 46 hr, an average of 33 more motor neurons label in the wild-type mice than the early symptomatic transgenic mice of the same age group (t-test, *$p < 0.01$). Scale bar is 50 μm.

but none addresses the underlying cause for the specificity of disease in motor neurons, the late onset of the disease, and the cumulative progressive nature of the disease. Deficiencies or interruptions in axonal transport have been previously proposed to lead to degeneration of affected motor neurons. This is not unreasonable, because motor neurons are large cells with extensively long axons that rely heavily on the transport of organelles and cytoskeletal proteins for the health and maintenance of the cell. In fact, transgenic mouse models of known FALS mutations, such as the SOD-1 mutant, have been examined for axonal transport deficiencies. Decreased transport times of cargo in both slow and fast anterograde transport have been found weeks before the onset of clinical symptoms (Cleveland, 1999). The dynamitin-overexpressing transgenic mouse model we report here addresses the question of whether a specific targeted disruption of microtubule-based transport is sufficient to recapitulate a motor neuron degenerative disease.

Overexpression of dynamitin has been a powerful tool in the elucidation of the cellular functions of dynein and dynactin. Previous experiments performed in vitro or in transfected tissue culture cells have demonstrated that elevated dynamitin levels lead to the specific disruption of the dynactin complex and the interruption of several dynein-mediated cellular functions, including minus-end-directed microtubule transport (Echeverri et al., 1996; Burkhardt et al., 1997; Presley et al., 1997; Eckley et al., 1999). Here we describe a transgenic mouse overexpressing dynamitin, leading to significant disruption of dynactin in the motor neurons of the spinal cord. We have achieved high levels of motor neuron-specific dynamitin expression using the Thy1.2 expression cassette, with significant protein levels observed after postnatal day 13. This postdevelopmental onset of transgene expression allowed us to focus on the role of transport in mature neurons, in contrast to previous studies in *Drosophila* (Reddy et al., 1997) and mice (Harada et al., 1998), which demonstrated a key role for dynein/dynactin in development.

Dynein is a unidirectional motor responsible for retrograde vesicle transport along microtubules. While dynein is not thought to have an active role in anterograde fast transport, previous studies have shown a link between plus-end- and minus-end-directed motors. For example, in extruded squid axoplasm, blocking the interaction of dynein and dynactin was observed to result in a bidirectional block in vesicle transport along microtubules (Waterman-Storer et al., 1997). A similar bidirectional inhibition of motility was induced using anti-kinesin antibodies (Brady et al., 1990). In *Drosophila*, genetic interactions between dynein, dynactin, and kinesin have been observed, also resulting in a bidirectional inhibition of axonal transport (Martin et al., 1999).

Dynein and dynactin have also been proposed to have a role in slow anterograde transport (Dillman et al., 1996), but their exact function, as well as the mechanism of slow transport, remains unknown. Dynein and dynactin have been found to be associated with isolated neurofilaments and to catalyze the transport of these filaments along microtubules in vitro (Shah et al., 2000). Recent live cell imaging of cultured neurons transfected with GFP-labeled neurofilament M subunit has suggested that the net velocity of neurofilament slow transport is actually comprised of fast anterograde transport that is interrupted by either pauses or retrograde movements (Wang et al., 2000). Net slow transport of these filaments down the axon may result from the dual activity of the opposing motors kinesin and dynein.

Therefore, it is conceivable that disruption of dynein/dynactin would essentially eliminate slow transport be-

cause of the nonopposition to kinesin, and all anterograde transport would then be at fast rates, including the transport of neurofilaments. This would account for the accumulation of neurofilaments observed in axons of affected neurons rather than more proximally or in the cell body, reflecting a specific defect in dynein/dynactin-mediated transport. An interesting possibility is that the saltatory retrograde movements that Wang et al. (2000) saw when observing NF transport were performing a function critical to NF transport rather than merely reflecting the result of inefficient transport. The long pauses and retrograde movements of NFs seen may result from the necessity to "space out" the transport of these large polymers down the axon, thus relieving steric hindrance to further transport. The upward trend in the variability of axonal caliber seen in early symptomatic transgenic mice (Figure 7D) may be the result of a loss of caliber maintenance resulting from inhibited retrograde function. The drop out of large caliber axons observed in late symptomatic mice would then demonstrate the critical role this loss of maintenance has on axonal survival.

Transgenic mice in the M21 line do not develop overt clinical signs until 5–9 months of age, and the onset of disease is variable. The rate of decline between littermates is also variable, often with episodes of decline and improvement. Mice typically display initial minor spontaneous fine muscle tremors that progress over time to more violent, spastic tremors. Hind limb weakness is commonly seen, resulting in decreased rearing activity, difficulty walking, occasional hopping with both hind limbs, and decreased stride length. Forelimb weakness is also seen, but less commonly. Although the presentation and onset of clinical signs in these mice are more variable than that seen in the SOD-1 mouse model, they may more closely resemble the clinical presentation of the spontaneous form of ALS in humans than do previous animal models.

One possibility for the observed variability of clinical signs associated with the overexpression of dynamitin may be compensation at the cellular level. Overexpressed dynamitin could be sequestered in some fashion by the upregulation of another dynactin subunit, p22. Supporting this theory is the observation that complete fragmentation of dynactin results in the partitioning of p22 and dynamitin in the same fraction of sucrose gradients (Eckley et al., 1999). Preliminary data suggest that levels of p22 expression vary inversely with the severity of phenotype observed. Another possibility to explain the variation in phenotype seen in these mice could be the variation of transgene expression seen in motor neurons. Although expression is very specific and high in motor neurons, not every motor neuron displays high levels of transgene expression. This variation of Thy1.2 expression in subsets of motor neurons has been previously observed (Feng et al., 2000). While denervation of a muscle fiber would result in its degeneration, that fiber could recover if it was reinnervated by sprouting from a neighboring healthy motor neuron. Until the number of motor neurons affected begins to compromise the innervation of the entire muscle, an overt phenotype will not be displayed.

Deficiencies in axonal transport have long been postulated to initiate degeneration of motor neurons, which rely extensively on microtubule-based transport for their survival. Previous studies on transgenic mouse models of FALS have found defects in axonal transport, but the question remained whether defective transport is sufficient to cause the disease. In this report, we describe a clear connection between the disruption of dynein/dynactin by the overexpression of dynamitin, decreased retrograde transport times of a neuro-tracer cargo, and the degeneration of motor neurons and their axons with the development of a phenotype consistent with a motor neuron degenerative disease. In this mouse model, overexpression of dynamitin inhibits but does not completely eliminate retrograde transport. This inhibition results in cumulative damage to the motor neuron, leading to degeneration and eventual cell death. Further characterization of the interplay between inhibition of transport and neuronal degeneration in these mice, as well as the potential compensatory sprouting and regeneration that prolong the disease time course in the dynamitin transgenic mice, should provide additional insight into the specific roles of dynein and dynactin as well as provide further understanding of the underlying mechanisms for the pathogenesis of motor neuron loss observed in diseases such as ALS.

Experimental Procedures

Generation of Transgenic Mice

The full-length human cDNA encoding dynamitin was obtained from the ATCC as previously described (Karki et al., 1998). The cDNA was modified by PCR using the primers p505′ (TAGCTCGAGCCATG GCGGACCCTAAATACGC) and p503′ (TAGCTCGAGTCACTTGTCG TCATCGTCTTTGTAGTCCTTTCCCAGCTTCTTCATCCGTTCATCAA TGC) to include a C-terminal FLAG tag to facilitate the identification of the transgene. The resulting construct was subcloned into the XhoI site of the Thy1.2 mouse expression cassette (a generous gift of P. Caroni), generating pThy1.2p50flag (Figure 1A). The EcoRI-PvuI fragment containing the expression cassette with the p50flag transgene was isolated from vector sequence and purified by gel electrophoresis, Qiaex purification, and passing over an Elutip ion exchange column (Schleicher & Shuell, Keene, NH). The DNA was then ethanol precipitated, resuspended in injection buffer (10 mM Tris/0.1 mM EDTA [pH 7.5]) at a concentration of 1–5 μg/μl, and submitted to the Transgenic Facility at the University of Pennsylvania School of Medicine for injection into fertilized C57BL/6 homozygous mouse eggs.

Positive offspring were identified by PCR of tail biopsies using the 5′ primer DH16 (CTTGGACCTCATGCAGTAGG) and the 3′ primer pu2p50 (GGATCTCCAGCCCTCAAG). Fourteen mice were shown to be positive for the transgene. These mice were then screened for germline integration of the transgene by backcrossing with B6SJL/F1 mice (Jackson Labs, Bar Harbor, ME), which were chosen for hybrid vigor, and three mice (M5, M13, and M21) were identified as founders. All of the animals used in these studies were kept in a pathogen-free environment, and the experimental procedures were approved by the IACUC committee at the University of Pennsylvania.

RNase Protection Assays

RNase protection assays were performed to quantify the levels of dynamitin expression in transgenic mice. RNA was isolated from mouse brains using the RNAwiz kit (Ambion, Austin, TX) according to the manufacturer's instructions. RNA was prepared from age-matched negative mice and representatives from the three lines of founder mice. The DNA probe was prepared from an antisense clone of the PCR product using the primers DH16 and pu2p50 from pThy1.2p50. The probe was labeled using the RPA II kit from Ambion and [α-^{32}P]UTP. Approximately 1.5 $\times$ 10^6 dpm of labeled RNA was added to each sample and incubated in the hybridization buffer overnight at 45°C.

RNase of the hybridization mixture was done according to manufacturer's directions, and the resulting product resolved on a 5% polyacrylamide/8 M urea gel. Gels were dried down under vacuum at 75°C for 60 min onto filter paper (Fisher, Pittsburgh, PA) and exposed overnight to X-Omat Blue film (Kodak, Rochester, NY) with double intensifying screens at −80°C. Levels of expression were determined by analysis of the blot by NIH Image.

Biochemical Characterization of Dynamitin and Dynactin in Wild-Type and Transgenic Mice

Western analysis of transgenic and wild-type mouse tissues was done to determine the onset and pattern of Thy1.2p50flag expression. Brain and spinal cord extracts were prepared by homogenization in buffer A (50 mM Tris-HCl [pH 7.4], 150 mM NaCl, 1 mM EDTA) plus protease inhibitors (AEBSF, aprotinin, leupeptin, pepstatin A, TAME) (Echeverri et al., 1996) and resolved on 10% SDS-PAGE gels. Gels were transferred to Immobilon-P membranes, blocked in 5% non-fat dry milk in TBS plus 0.5% Igepal, and probed with the monoclonal antibodies anti-kinesin (Chemicon, Temecula, CA), anti-dynamitin (Transduction Labs, San Diego, CA), and anti-FLAG (Sigma, St Louis, MO). Polyclonal antibodies used were anti-Arp1 (Holleran et al., 1996), anti-p150^{Glued} (Melloni et al., 1995), anti-p22 (Karki et al., 1998), and anti-p62 (Karki et al., 2000). An anti-dynamitin polyclonal antibody was produced as previously described for p150^{Glued} (Tokito et al., 1996). Rabbits were immunized using the recombinant full-length human dynamitin. Antibodies were affinity purified from the serum against the antigen.

Tissues screened were forebrain, midbrain, cerebellum, brain stem, spinal cord, heart, lung, liver, spleen, testes, uterus, ovaries, and forelimb and hind limb muscles from the wild-type and transgenic mice. Tissues were homogenized in buffer B (20 mM Tris-HCL [pH 7.4], 2 mM EGTA, 1 mM EDTA) plus protease inhibitors (leupeptin, pepstatin A, TAME, and PMSF). Homogenates were resolved by 8% SDS-PAGE as described above, transferred to Immobilon-P membranes, blocked with 5% milk solution, and probed with polyclonal anti-dynamitin. Visualization was done with the non-radioactive Renaissance kit (NEN, Boston, MA) according to the manufacturer's directions.

High-speed supernatants were made from spinal cord homogenates of 5-month-old presymptomatic transgenic and wild-type mice in buffer A plus protease inhibitors and fractionated on sucrose gradients. Approximately 200 μl of homogenates was overlaid onto a 12 ml, 5%–20% sucrose gradient and centrifuged at 32 K for 18 hr. Simultaneously, gradients loaded with the markers aldolase, catalase, BSA, thyroglobulin, and lysozyme were run in parallel as standards to determine the 20S and 4S fractions. One milliliter fractions were collected from each gradient and resolved by 10% SDS-PAGE. Gels were transferred to Immobilon-P membranes, blocked with 5% milk solution, and probed with the monoclonal antibodies to tubulin, actin, the FLAG tag, and the polyclonal antibodies anti-Arp1, anti-p150^{Glued}, anti-p22, anti-dynamitin, and anti-p62.

Characterization of Transgenic Phenotype

Mice were regularly monitored to assess the onset, severity, and progression of symptoms associated with transgene expression. Mice were examined by a veterinarian to determine the phenotype and assigned a score of 0 to 5, concurrent with severity. Mice with a score of 0 did not show any clinical signs while a 5 indicated paralysis. Mice were euthanized when they were determined to have a significant loss of weight, indicating an inability to reach food, or when they became moribund. All transgenic mice used in these experiments were categorized into presymptomatic, early symptomatic, or late symptomatic to normalize the extent of clinical signs of the mice used in the experiments. Presymptomatic mice are defined as being 4- to 7-month-old and have a phenotype score of 0. Early symptomatic mice are 10- to 14-month-old and have a phenotype score of 1–2, whereas late symptomatic mice are 17-month-old and older and have a phenotype score of 3–4. Stride length was analyzed by placing the mice in a one-directional chute laid with paper following painting of their feet with a nontoxic paint.

Treadmill tolerance tests of mice were done on a 6-lane belt-driven treadmill constructed for mice from Columbus Instruments (Columbus, OH). After acclimation to the instrument, male mice were exercised with the treadmill incline set at 20° until determined to be exhausted by their refusal to run despite short resting periods (<1 min rests on platform) and gentle prodding with a tongue depressor. Mice were started at a belt speed of 9 m/min for 20 min and then progressed to 12 m/min up to 2 hr running time, after which mice were run at 17 m/min until refusal to run. This protocol of slow to moderate speeds was designed to test the endurance time of the mouse rather than the maximum speed that the mouse could run (Pagala et al., 1998). 4- to 7-month-old presymptomatic (phenotype score = 0, n = 8), 10- to 14-month-old early symptomatic (phenotype score = 1–2, n = 5), >17-month-old late symptomatic (phenotype score = 3–4, n = 6), and age-matched wild-type control mice were examined, mean running time and SE were calculated, the t test was applied, and p values of <0.02 were determined for mice in the 10- to 14-month-old and >17-month-old age groups.

In order to quantify the decrease in strength observed in symptomatic transgenic mice, a grip strength meter was used (Columbus Instruments) as previously described (Meyer et al., 1979, Zhao, et al., 2001). Briefly, male mice grasp a triangular ring that is connected to a tension digital force transducer and is gently pulled by the tail away from the bar that measures the maximum tension produced. Three trials are done consecutively on each mouse with no more than 30 s between each trial, and the three values are averaged and corrected for the weight of the mouse to produce a kg of tension produced per kg weight of the mouse. 4- to 7-month-old presymptomatic (phenotype score = 0, n = 41), 10- to 14-month-old early symptomatic (phenotype score = 1–2, n = 29), >17-month-old late symptomatic (phenotype score = 3–4, n = 7), and age-matched wild-type control mice were examined, mean tension/weight and SE were calculated, the t test was applied, and a p value of <0.001 was determined for mice in the >17-month-old age group.

Immunohistochemistry

Histology was performed on early and late symptomatic transgenic and age-matched negative control mice to further characterize the pathology produced from dynamitin overexpression in motor neurons. Tissues were fixed overnight in 10% formalin, paraffin embedded, and processed by standard protocols. Tissues screened were brain and spinal cord as well as thoracic and lumbar whole limbs. Sections were cut into 12 μm sections and stained with H&E (Fisher).

Immunohistochemistry was performed on 10- to 14-month-old early symptomatic transgenic and wild-type mice in parallel. Cross-sections of spinal cord formalin fixed, paraffin embedded slides were processed by standard protocols to dissolve paraffin, permeabilized with Proteinase K, and blocked with 0.03% hydrogen peroxide. Primary antibodies used were: mouse monoclonal anti-dynamitin (Chemicon) and rabbit polyclonals anti-neurofilament (M0762) and anti-synaptophysin (Dako, Carpinteria, CA). The anti-neurofilament polyclonal antibody M0762 recognizes the phosphorylated forms of the light and heavy subunits only. Antibodies were conjugated directly to horseradish peroxidase using the $LSAB_2$ kit from Dako according to the manufacturer's directions and visualized with DAP (Dako). Sections were counterstained with hemotoxylin. Histology and immunohistochemistry sections were processed and evaluated by the pathobiology department of the University of Pennsylvania School of Veterinary Medicine.

Electron Microscopy

Pre-, early, and late symptomatic dynamitin transgenic and age-matched control mice were deeply anesthetized with an intraperitoneal injection of ketamine/xylazine (1 mg/gm and 0.1 mg/gm), sacrificed by intracardiac perfusion, and their L5 ventral roots harvested and processed for EM analysis as previously described (Zhang et al., 1997). Briefly, mice were fixed by perfusion with 30–50 ml of 2% glutaraldehyde and 2% paraformaldehyde in 0.1 M cacodylate buffer. The L5 ventral roots were removed, postfixed in 1% osmium tetroxide for 20 min, and processed for embedding in Epon-Araldite resin. Ultrathin sections were cut, mounted in 100 mesh or open grids, and stained with 1% uranyl acetate and 0.5% lead citrate. Grids were analyzed with a 100CX Joel Electron Microscope at 80 kV.

Quantitation of L5 ventral roots was performed as in Bruijin et al. (1997). Mice were grouped as follows: 4- to 7-month-old wild-type (n = 2) and presymptomatic transgenic mice (n = 2), 10- to 14-

month-old wild-type (n = 2) and early symptomatic mice (n = 2), and >16-month-old wild-type (n = 3) and late symptomatic transgenic mice (n = 3). The total number of axons in the ventral roots was determined (t test, $p < 0.08$ for >16-month-old late symptomatic transgenic mice) and reported as a percentage of the total number of axons in age-matched control mice. Large (>5 μm in diameter) and small (<5 μm in diameter) axons were counted for transgenic mice in each age group (t test, $p < 0.02$ for the decrease in LCAs found in the >16-month-old late symptomatic transgenic mice) and reported as a percentage of the number of small or large axons found in wild-type mice in the same age group.

Fluoro-Gold Neurotracer Experiments

Ten- to fourteen-month-old early symptomatic and wild-type control mice were used for the determination of retrograde transport using the neurotracer fluoro-gold (FluoroChrome, Denver, CO). Mice were immobilized in a restraint tube (Harvard Apparatus, Holliston, MA), and the caudal aspect of the left lower hind limb was clipped and prepped. A small stab incision was made in the skin 2–3 mm long to expose the underlying muscle at the widest point of the lower limb (~7–10 mm distal to the femorotibial joint). A 10 μl Hamilton syringe was used to deliver 1 μl of a 2% solution of fluoro-gold (wt/vol) in 0.9% saline at a medial, central, and lateral site approximately 2 mm deep in the gastrocnemius muscle of the mouse. Mice were sacrificed at 44 and 46 hr by CO_2 inhalation, the lumbar intumescence of the spinal cord was harvested and fixed in 4% paraformaldehyde made in PBS and floated in 20% sucrose until the cords sank (usually overnight), and longitudinal sections were prepared by standard methods. Sections were visualized using an A2 filter on a Leica DMRB epifluorescence microscope, and the total number of motor neurons accumulating fluoro-gold in their cell bodies was counted for each mouse. The mean number of cell bodies accumulating fluoro-gold and SE was calculated for wild-type (n = 6) versus early symptomatic transgenic (n = 4) 10- to 14-month-old mice for the 44 hr and 46 hr time points.

Acknowledgments

The Thy1.2 expression vector was a generous gift from Pico Caroni. The authors gratefully acknowledge Bin Zhang, Neelima Shah, and the Biomedical Core Imaging Facility for their assistance in the EM studies, Jackie Farracone for her assistance with the immunohistochemistry, Zi-Shun Chao for his assistance with the fluoro-gold studies, Richard Miselis for his thoughtful contributions, as well as Sher Karki and Lee Ligon for their comments on the manuscript. This work was supported by the Amyotrophic Lateral Sclerosis Association, NIH GM48661, NIH GM56707, the Research Foundation of the University of Pennsylvania, and an Established Investigator Award to E.L.F.H. from the American Heart Association.

Received: March 9, 2001
Revised: March 25, 2002

References

Ahmed, F.J., Echeverri, C.J., Vallee, R.B., and Baas, P.W. (1998). Cytoplasmic dynein and dynactin are required for the transport of microtubules into the axon. J. Cell Biol. *140*, 391–401.

Borchelt, D.R., Wong, P.C., Sisodia, S.S., and Price, D.L. (1998). Transgenic mouse models of Alzheimer's disease and amyotrophic lateral sclerosis. Brain Pathol. *8*, 735–757.

Brady, S., Pfister, K., and Bloom, G. (1990). A monoclonal antibody against kinesin inhibits both anterograde and retrograde fast axonal transport in squid axoplasm. Proc. Natl. Acad. Sci. USA *87*, 1061–1065.

Bruijin, L.I., Becher, M.W., Lee, M.K., Anderson, K.L., Jenkins, N.A., Copeland, N.G., Sisodia, S.S., Rothstein, J.D., Borchelt, D.R., Price, D.L., and Cleveland, D.W. (1997). ALS-linked SOD1 mutant G85R mediates damage to astrocytes and promotes rapidly progressive disease with SOD1-containing inclusions. Neuron *18*, 327–338.

Burkhardt, J.K., Echeverri, C.J., Nilsson, T., and Vallee, R.B. (1997). Overexpression of the dynamitin (p50) subunit of the dynactin complex disrupts dynein-dependent maintenance of membrane organelle distribution. J. Cell Biol. *139*, 469–484.

Caroni, P. (1997). Overexpression of growth-associated proteins in the neurons of adult transgenic mice. J. Neurosci. Methods *71*, 3–9.

Cleveland, D.W. (1999). From Charcot to SOD1: mechanisms of selective motor neuron death in ALS. Neuron *24*, 515–520.

Collard, J.-F., Côte, F., and Julien, J.-P. (1995). Defective axonal transport in a transgenic mouse model of amyotrophic lateral sclerosis. Nature *375*, 61–64.

Dillman, J.F., III, Dabney, L.P., Karki, S., Paschal, B.M., Holzbaur, E.L.F., and Pfister, K.K. (1996). Functional analysis of dynactin and cytoplasmic dynein in slow axonal transport. J. Neurosci. *16*, 6742–6752.

Echeverri, C.J., Paschal, B.M., Vaughan, K.T., and Vallee, R.B. (1996). Molecular characterization of the 50-kD subunit of dynactin reveals function for the complex in chromosome alignment and spindle organization during mitosis. J. Cell Biol. *132*, 617–633.

Eckley, D.M., Gill, S.R., Melkonian, K.A., Bingham, J.B., Goodson, H.J., Heuser, J.E., and Schroer, T.A. (1999). Analysis of dynactin subcomplexes reveals a novel actin-related protein associated with the Arp1 minifilament pointed end. J. Cell Biol. *147*, 307–319.

Elder, G.A., Friedrich, V.L., Kang, C., Bosco, P., Gourov, A., Tu, P.-H., Lee, V.M.-Y., and Lazzarini, R.A. (1998a). Requirement of heavy neurofilament subunit in the development of axons with large calibers. J. Cell Bio1 *143*, 195–205.

Elder, G.A., Friedrich, V.L., Bosco, P., Kang, C., Gourov, A., Tu, P.-H., Lee, V.M.-Y., and Lazzarini, R.A. (1998b). Absence of the mid-sized neurofilament subunit decreases axonal calibers, levels of light neurofilament (NF-L), and neurofilament content. J. Cell Biol. *141*, 727–739.

Feng, G., Mellor, R.H., Bernstein, M., Keller-Peck, C., Nguyen, G.T., Wallace, M., Nerbonne, J.M., Lichtman, J.W., and Sanes, J.R. (2000). Imaging neuronal subsets in transgenic mice expressing multiple spectral variants of GFP. Neuron *28*, 41–51.

Harada, A., Takei, Y., Kanai, Y., Tanaka, Y., Nonaka, S., and Hirokawa, N. (1998). Golgi vesiculation and lysosome dispersion in cells lacking cytoplasmic dynein. J. Cell Biol. *141*, 51–59.

Hirokawa, N., Sato-Yoshitake, R., Yoshida, T., and Kawashima, T. (1990). Brain dynein (MAP1C) localizes on both anterogradely and retrogradely transported membranous organelles in vivo. J. Cell Biol. *111*, 1027–1037.

Holleran, E.A., Tokito, M.K., Karki, S., and Holzbaur, E.L.F. (1996). Centractin (ARP1) associates with spectrin revealing a potential mechanism to link dynactin to intracellular organelles. J. Cell Biol. *135*, 1815–1829.

Holleran, E.A., Ligon, L.A., Tokito, M., Stankewich, M.C., Morrow, J.S., and Holzbaur, E.L.F. (2001). βIII Spectrin binds to the Arp1 subunit of dynactin. J. Biol. Chem. *276*, 36598–36605.

Julien, J.P. (1997). Neurofilaments and motor neuron disease. Trends Cell Biol. *7*, 243–249.

Julien, J.P. (2001). Amyotrophic lateral sclerosis: unfolding the toxicity of the misfolded. Cell *104*, 581–591.

Karki, S., and Holzbaur, E.L.F. (1995). Affinity chromatography demonstrates a direct binding between cytoplasmic dynein and dynactin complex. J. Biol. Chem. *270*, 28806–28811.

Karki, S., LaMonte, B., and Holzbaur, E.L.F. (1998). Characterization of the p22 subunit of dynactin reveals the localization of cytoplasmic dynein and dynactin to the midbody of dividing cells. J. Cell Biol. *142*, 1023–1034.

Karki, S., Tokito, M.K., and Holzbaur, E.L.F. (2000). A dynactin subunit with a highly conserved cysteine-rich motif interacts directly with Arp1. J. Cell Biol. *275*, 4834–4839.

King, S.J., and Schroer, T.A. (2000). Dynactin increases the processivity of the cytoplasmic dynein motor. Nat. Cell Biol. *2*, 20–24.

Li, J.-Y., Pfister, K., Brady, S.T., and Dahlström, A. (2000). Cytoplasmic dynein conversion at a crush injury in rat peripheral axons. J. Neurosci. Res. *61*, 151–161.

Martin, M.A., Iyadurai, S.J., Gassman, A., Gindhart, J.G., Hays, T.S., and Saxton, W.M. (1999). Cytoplasmic dynein, the dynein complex

and kinesin are interdependent and essential for fast axonal transport. Mol. Biol. Cell *10*, 3717–3728.

Melloni, R.H., Tokito, M.K., and Holzbaur, E.L.F. (1995). Expression of the p150Glued component of the dynactin complex in developing and adult rat brain. J. Comp. Neurol. *357*, 15–24.

Meyer, O.A., Tilson, H.A., Byrd, W.C., and Riley, M.T. (1979). A method for the routine assessment of fore- and hindlimb grip strength of rats and mice. Neurobehav. Toxicol. *1*, 233–236.

Muresan, V., Stankewich, M.C., Steffen, W., Morrow, J.S., and Schnapp, B.J. (2001). Dynactin-dependent, dynein-driven vesicle transport in the absence of membrane proteins: a role for spectrin and acidic phospholipids. Mol. Cell *7*, 173–183.

Murphey, R.K., Caruccio, P.C., Getzinger, M., Westgate, P.J., and Phillis, R.W. (1999). Dynein-dynactin function and sensory axon growth during *Drosophila* metamorphosis: a role for retrograde motors. Dev. Biol. *209*, 86–97.

Navone, F., Jahn, R., Di Gioia, G., Stukenbrok, H., Greengard, P., and De Camilli, P. (1986). Protein p38: an integral membrane protein specific for small vesicles of neurons and neuroendocrine cells. J. Cell Biol. *103*, 2511–2527.

Pagala, M., Ravindran, K., Namba, T., and Grob, D. (1998). Skeletal muscle fatigue and physical endurance of young and old mice. Muscle Nerve *21*, 1729–1739.

Paschal, B.M., and Vallee, R.B. (1987). Retrograde transport by the microtubule associated protein MAP 1C. Nature *330*, 181–183.

Presley, J.F., Cole, N.B., Schroer, T.A., Hirschberg, K., Zaal, K.J.M., and Lippincott-Schwartz, J. (1997). ER-to-Golgi transport visualized in living cells. Nature *389*, 81–85.

Reddy, S., Jin, P., Trimarchi, J., Caruccio, P., Phillis, R., and Murphey, R.K. (1997). Mutant molecular motors disrupt neural circuits in Drosophila. J. Neurobiol. *33*, 711–723.

Rosen, D.R., Siddique, T., Patterson, D., Figlewicz, D.A., Sapp, P., Hentati, A., Donaldson, D., Goto, J., O'Regan, J.P., Deng, H.X., et al. (1993). Mutations in Cu/Zn superoxide dismutase gene are associated with familial amyotrophic lateral sclerosis. Nature *362*, 59–62.

Schmued, L. (1994). Anterograde and retrograde tract tracing with fluorescent compounds within the CNS. Elsevier's Neuroscience Protocols *50*, 1–15.

Shah, J.V., Flanagan, L.A., Janmey, P.A., and Leterrier, J.-F. (2000). Bidirectional translocation of neurofilaments along microtubules mediated in part by dynein/dynactin. Mol. Biol. Cell *11*, 3495–3508.

Starr, D.A., Williams, B.C., Hays, T.S., and Goldberg, M.L. (1998). ZW10 helps recruit dynactin and dynein to the kinetochore. J. Cell Biol. *142*, 763–774.

Tokito, M.K., Howland, D.S., Lee, V.M.-Y., and Holzbaur, E.L.F. (1996). Functionally distinct isoforms of dynactin are expressed in human neurons. Mol. Biol. Cell *7*, 1167–1180.

Wang, L., Ho, C., Sun, D., Liem, R.K.H., and Brown, A. (2000). Rapid movement of axonal neurofilaments interrupted by prolonged pauses. Nat. Cell Biol. *2*, 137–141.

Waterman-Storer, C.M., Karki, S., and Holzbaur, E.L.F. (1995). The $p150^{Glued}$ component of the dynactin complex binds to both microtubules and the actin-related protein centractin (Arp1). Proc. Natl. Acad. Sci. USA *92*, 1634–1638.

Waterman-Storer, C.M., Karki, S., Kuznetsov, S.A., Tabb, J.S., Weiss, D.G., Langford, G.M., and Holzbaur, E.L.F. (1997). The interaction between cytoplasmic dynein and dynactin is required for fast axonal transport. Proc. Natl. Acad. Sci. USA *94*, 12180–12185.

Williamson, T.L., and Cleveland, D.W. (1999). Slowing of axonal transport is a very early event in the toxicity of ALS-linked SOD1 mutants to motor neurons. Nat. Neurosci. *2*, 50–56.

Xu, Z., Marszalek, J.R., Lee, M.K., Wong, P.C., Folmer, J., Crawford, T.O., Hsieh, S.-T., Griffin, J.W., and Cleveland, D.W. (1996). Subunit composition of neurofilaments specifies axonal diameter. J. Cell Biol. *133*, 1061–1069.

Yang, Y., Hentati, A., Deng, H.-X., Dabbagh, O., Sasaki, T., Hirano, M., Hung, W.-Y., Ouahchi, K., Yan, J., Azim, A.C., et al. (2001). The gene encoding alsin, a protein with three guanine-nucleotide exchange factor domains, is mutated in a form of recessive amyotrophic lateral sclerosis. Nat. Genet. *29*, 160–165.

Zhang, B., Tu, P., Abtahian, F., Trojanowski, J.Q., and Lee, V.M.-Y. (1997). Neurofilaments and orthograde transport are reduced in ventral root axons of transgenic mice that express human SOD1 with a G93A mutation. J. Cell Biol. *139*, 1307–1315.

Zhao, C., Takita, J., Tanaka, Y., Setou, M., Nakagawa, T., Takeda, S., Yang, H.W., Terada, S., Nakata, T., Takei, Y., et al. (2001). Charcot-Marie-Tooth disease type 2A caused by a mutation in a microtubule motor KIF1Bβ. Cell *105*, 587–597.